Fundaments in Luminance and Retroreflectivity Measurements of Vertical Traffic Signs Using a Color Digital Camera

Philip Siegmann, Roberto Javier López-Sastre, Pedro Gil-Jiménez, Sergio Lafuente-Arroyo, and Saturnino Maldonado-Bascón, *Member, IEEE*

***Abstract*—This paper is a study of the influences of the different parameters which affect the photometric evaluation of light-emitting surfaces (due to reflection or self- emission) when a conventional color digital camera is used. The overall purpose of this paper is to evaluate the luminance and the reflectivity of the vertical traffic sign with the camera in order to provide an automatic recognition of deteriorated reflective sheeting material of which the traffic signs were made. This paper describes how the A/D converter output signal given by a pixel of the digital camera can be related to the luminance and the reflectivity of the corresponding surface element whose image is formed on a pixel. Thus, each surface element of the traffic sign's surface can be separately evaluated. By photometrically calibrating the camera, we have been able to prove this relationship in our experiments.**

***Index Terms*—Calibration, CMOS image sensor, digital camera, luminance, photometry, reflectivity, retroreflectivity.**

I. Introduction

THERE IS no doubt about the importance of maintaining vertical traffic-sign visibility for both the safety and orientation reasons of road users. By visibility, we mean the ability of a person to see and extract useful information from the sign. This ability encompasses many different considerations and is therefore difficult to quantify [1]. In summary, we can say that there is good visibility if there is a marked contrast. To provide night-time visibility, traffic signs are mostly made of retroreflective sheeting material which improves the brightness contrast between the sign and its background when they are illuminated. In order to also provide day-time visibility and message identification, different colors and reflective capacity are used, which improve both the color and the brightness contrast within the sign. We focused this paper on a photometric evaluation using a calibrated digital color camera so that we could associate each color with the corresponding weight of the human-eye sensitivity [2]–[4]. The advantage of using a digital camera for sign visibility evaluation is the possibility of measuring their uniformity over the whole surface, allowing the evaluation of the legibility of the message and the facility to make the process automatic. For an automatic sign visibility evaluation, a previous detection and recognition of the sign within the image of the road is necessary. This can be performed using support vector machines [5].

The closest measurable parameter to evaluate the brightness of the traffic sign at night is the luminance, which is defined as the luminous energy flow in a spatial direction emitted by a surface element perpendicular to this direction, but it is not a reliable parameter to analyze the deterioration of reflective sheeting-material because of the strong influence of the light which illuminates the sign. However, the reflectivity, which is defined as the luminance divided by the luminous energy flow impinging on a surface element (i.e., illuminance), is a parameter which is more closely related to the surface deterioration, but it is still influenced by the relative orientation between the light source, the sign, and the camera. An example of the complexity of the involved geometry can be seen in [6], where a study of the reflection properties of road surfaces is presented. To overcome this last influence of the relative orientation and to find a parameter which almost only depends on the surface deterioration of the sign, we need to know how the surface reflects the light, or alternatively, we need to establish a specific relative orientation between light source–sign–camera. When the sign surface is illuminated and framed from the same place, the measured reflectivity is called the retroreflectivity, which finally constitutes the established parameter used for the evaluation of the sheeting-material deterioration of the traffic sign [1], [7]. Furthermore, the sheeting material is supposed to be retroreflective. In this case, the surface orientation with respect to the incident light beam may not have a great influence on the retroreflectivity measurement.

The correspondence between the signal obtained from a color digital camera at each pixel and the luminance emitted from the sign to the camera is obviously related to the camera settings (exposure time, aperture number, and focal length) and to the digital response of the photodetector (typically, a charge-coupled device (CCD) or, as in our case, a CMOS matrix). The CCD sensor has a linear response [2]–[4], [6], whereas the CMOS photodetector that we used exhibited a nonlinear response to the amount of luminous energy impinging on it. The principal advantage of using the CMOS photodetector is that there will be no blooming effect so that the saturated pixels will not affect their neighbors. To determine the response of

Manuscript received May 4, 2006; revised September 30, 2007. This work was supported by the Ministerio de Educación y Ciencia of Spain under Project TEC2004/03511/TCM.

The authors are with the Department of Signal Theory and Communications, Universidad de Alcalá, 28801 Alcalá de Henares, Spain (e-mail: philip.siegmann@uah.es; saturnino.maldonado@uah.es).

Digital Object Identifier 10.1109/TIM.2007.911643

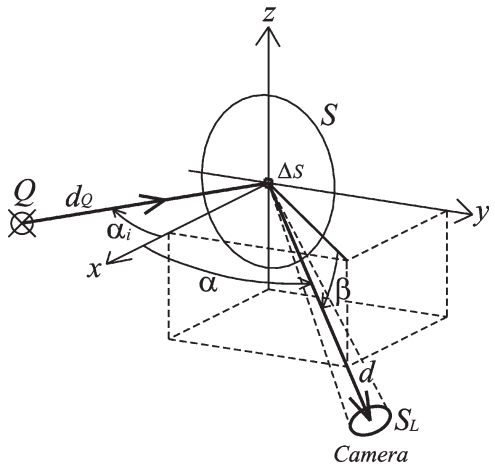

Fig. 1. Reference coordinate system for the surface element ΔS illuminated by the light source Q and viewed by the camera with an entrance pupil S_{L}.

the camera (photodetector with an objective) to different light energies and colors, we have done a photometrical calibration of the camera using a luxometer and an intensity variable diffuse light screen source. By examining each pixel, we find that our camera shows a nonlinear variation in each of the pixel's responses or an A/D converter output with the incident light energy, and they are similar for the red, green, and blue lights detected by each channel. This results in a specific photometrical response function (equivalent to the luminance calibration coefficient for the case of CCDs) for the color CMOS camera that includes the nonlinear response of the photodetector and the visibility factor for the different colors that appear on the traffic signs.

II. Background

For the analysis of the photometrical parameters [7], [8] involved in our problem of a surface (S) illuminated by a light source (Q) and observed with a camera with an entrance pupil (S_{L}), we consider the reference coordinate system shown in Fig. 1. The origin of the coordinate system is placed on the sign surface element (ΔS) from which we are going to measure the emitted luminous flux into the camera. The x-axis coincides with the normal to the surface, and the y-axis is placed on the plane defined by the incident light beam and the x-axis (i.e., plane of incidence). The distance between the light source and the surface element is marked with d_Q, and the distance from the surface element to the camera is marked with d. The incident angle (α_{i}) is sufficient to define the incident beam direction onto the element surface in our coordinate system, and the angles that define the emission direction to the camera are designated with α and β, where α is the angle between the x-axis and the emission direction, and β is the angle between the plane of incidence and the emission direction.

By using the previously defined angles in our reference coordinate system, we have the direction of a specular reflection when $\alpha = -\alpha_{\mathrm{i}}$ and $\beta = 0$ and the direction of a retroreflection when $\alpha = \alpha_{\mathrm{i}}$ and $\beta = 0$. For a uniform diffuser, the emitted luminous intensity (I) is given by the Lambertian distribution

$$I(\alpha_{\mathrm{i}}; \alpha, \beta) = I(\alpha) = I_{\perp} \cos\alpha \tag{1}$$

where $I_{\perp}$ is the reflected intensity in a direction normal to the surface.

When illuminated with a light beam impinging on it with the incidence angle (α_{i}) and emitting the intensity $I_{\Delta S}$, the luminance (L) of a surface element (ΔS) in the direction of the observer (α, β) is given by

$$L(\alpha_{\mathrm{i}}; \alpha, \beta) = I_{\Delta S}(\alpha_{\mathrm{i}}; \alpha, \beta)/(\Delta S \cos\alpha) \tag{2}$$

and the illuminance (E_{i}) of the surface element illuminated by a point source of luminous intensity I_Q is given by

$$E_{\mathrm{i}} = I_Q w_{\Delta S}/\Delta S \tag{3}$$

where $w_{\Delta S}$ is the solid angle from the point source seen by the surface element (ΔS), and $F_{\mathrm{i}} = I_Q w_{\Delta S}$ is the incident energy flux on the surface element. The solid angle $w_{\Delta S}$ is given by

$$w_{\Delta S} = \Delta S \cos\alpha_{\mathrm{i}}/d_Q^2 \tag{4}$$

and is supposed to be the same over the whole sign surface whenever the light source is far enough from it. The reflectivity (R) of the surface element is defined as the luminance divided by the illuminance. With (2)–(4), we obtain

$$R(\alpha_{\mathrm{i}}; \alpha, \beta) = \frac{L(\alpha_{\mathrm{i}}; \alpha, \beta_{\mathrm{i}})}{E_{\mathrm{i}}} = \frac{I_{\Delta S}(\alpha_{\mathrm{i}}; \alpha, \beta_{\mathrm{i}})}{I_Q \cos\alpha_{\mathrm{i}} \cos\alpha} \cdot \frac{d_Q^2}{\Delta S}. \tag{5}$$

Our proposal is then to find out how the luminance and the reflectivity are measured with a digital camera and how these two elements depend on the camera settings and the illumination conditions.

III. Luminance and Reflectivity Measurements With the Digital Camera

As shown in Fig. 2, we consider the sign centered on the optical axis of the objective of the camera. This is the case when we direct the camera to the sign. To measure the luminance emitted from the surface element toward the camera, we equalize the luminous energy flux (F_{L}), which crosses the entrance pupil (S_{L}) of the camera with the luminous flux (F_{p}), which impinges on a pixel. The surface element (ΔS) is then defined as the one that forms image on the pixel (S_{p}).

Considering then that the camera is oriented to the sign and is far enough from it, we obtain the following for the luminous energy flux which crosses S_{L}:

$$\begin{aligned} F_{\mathrm{L}} &= I_{\Delta S}(\alpha_{\mathrm{i}}; \alpha, \beta) \cdot w_{\mathrm{L}} \\ &= L(\alpha_{\mathrm{i}}; \alpha, \beta) \cdot \Delta S \cos\alpha \cdot S_{\mathrm{L}}/d^2 \end{aligned} \tag{6}$$

where the solid angle w_{L} defined by S_{L} for each surface element is practically the same over the surface S when $d \gg$ dimensions of S. If the camera was not oriented toward the sign,

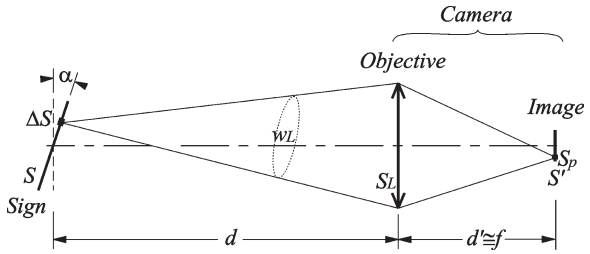

Fig. 2. Simplified diagram of the ray tracing between the sign surface and the photodetector. S, S_{L}, and S' are the sign surface, the entrance pupil, and the sensor surface, respectively. S_{p} is the image of ΔS. We suppose that $d \gg f$; hence, $d' \cong f$ (for simplicity on the figure, $\beta = 0°$).

an additional inclination or tilt factor would be necessary in (6), accounting for the lower energy flux entering the entrance pupil.

During the exposure time, the amount of luminous energy arriving at the pixel is a function of the A/D converter output signal (designed with n_{R}, n_{G}, and n_{B} for the different channels if a color camera is used or with n_{g} when only one channel is used). The energy flux which impinges on the pixel is then

$$F_{\mathrm{p}} = T_{\mathrm{exp}}^{-1} \cdot g(n_{\mathrm{g}}) \tag{7}$$

where T_{exp} is the exposure time, and $g(n_{\mathrm{g}})$ is defined as the photometrical response function of the camera. This function is experimentally obtained in the next paragraph and translates the A/D converter signal into lumens $\times$ second.

By equalizing (6) with (7), we obtain this for the luminance

$$L(\alpha_{\mathrm{i}}; \alpha, \beta) = \frac{g(n_{\mathrm{g}})}{T_{\mathrm{exp}} \Delta S \cos\alpha \cdot S_{\mathrm{L}}} d^2 \tag{8}$$

where we can substitute $\Delta S \cos\alpha = (S_{\mathrm{p}}/M)$, $M = (f/(d - f))^2$, and $S_{\mathrm{L}} = \pi(f/(2N_f))^2$, where M is the square of the lateral magnification, N_f is the aperture number, f is the focal length, and d is the distance between the sign surface and the camera. We need to take into account that the entrance pupil may not lie on the first lens of the objective, as shown in the simplified Fig. 2. Furthermore, we consider that $f/d \ll 1$; hence, the luminance simply depends on

$$L(\alpha_{\mathrm{i}}; \alpha, \beta) \cong \frac{4}{\pi} \frac{N_f^2}{T_{\mathrm{exp}} S_{\mathrm{p}}} g(n_{\mathrm{g}}). \tag{9}$$

Equation (9) gives the luminance of the surface element which forms an image on a pixel. For $f/d \ll 1$, there is no direct dependence with d. This can be explained because the size of the emitting surface element increases with the same rate with the distance to the camera ($\propto d^2$) as the luminous flux arriving at the pixel decreases ($\propto d^{-2}$).

With (5) in (9), we obtain the following for the reflectivity:

$$R(\alpha_{\mathrm{i}}; \alpha, \beta) \cong \frac{4}{\pi} \cdot \underbrace{\frac{N_f^2 g(n_{\mathrm{g}})}{T_{\mathrm{exp}} S_{\mathrm{p}}}}_{\text{camera}} \cdot \underbrace{\frac{d_Q^2}{I_Q \cos\alpha_{\mathrm{i}}}}_{\text{light source}}. \tag{10}$$

Here, we also have to know the lighting parameters: the intensity of the point light source toward the surface element, the distance from the light source to the surface, and the incident angle (i.e., the illuminance on the surface element).

IV. Photometrical Calibration of the Camera

The color digital camera that we use (Canon EOS 300D) has a 3072 $\times$ 2048 CMOS matrix sensor with a primary color filter for red (R), green (G), and blue (B) lights. The adjustable ISO sensitivity of the sensor has been fixed to 100. The response of each channel to the luminous energy of primary colors is given in n_{R}, n_{G}, and n_{B} values (short $n_{\mathrm{R,G,B}}$) with integer values lying between 0 and 255. The calibration for the CMOS sensor is done together with the objective (Canon ESF 18 : 55 mm, focal variable). To simplify the calibration process, we considered that each pixel has the same photometrical response function. Our aim is not a precise photometrical calibration but a good estimation of the luminance value measured with the camera, which is sufficient for the purpose of validating (9).

To obtain the luminous flux at a pixel from the camera in photometrical units (lumen) for a specific color, we use the Abney law for summation of the partial luminous flux of the primary colors ($\Phi_{\mathrm{R}}, \Phi_{\mathrm{G}},$ and Φ_{B}) measured by the camera (in watts) [7], [8]

$$683 \cdot F_{\mathrm{p}}(\mathrm{lm}) = V_{\mathrm{R}}\Phi_{\mathrm{R}}(W) + V_{\mathrm{G}}\Phi_{\mathrm{G}}(W) + V_{\mathrm{B}}\Phi_{\mathrm{B}}(W) \tag{11}$$

where $V_{\mathrm{R,G,B}}$ are the visibility factors for each of the primary colors, and 1 W of maximum visibility factor is 683 lumens. The visibility factors for the primary colors are not known *a priori* and need to experimentally be obtained, as we will explain later.

The luminous energy arriving at a pixel gives rise to a response of the camera in $n_{\mathrm{R,G,B}}$ values according to a response function that we want to determine. This response function may be different for each channel; thus, we define such a function for a pixel and for each of the channels $(\gamma_{\mathrm{R}}(n_{\mathrm{R}}), \gamma_{\mathrm{G}}(n_{\mathrm{G}}), \gamma_{\mathrm{B}}(n_{\mathrm{B}}))$ excited by the corresponding luminous flux as

$$\begin{aligned} \gamma_{\mathrm{R}}(n_{\mathrm{R}}) &= T_{\mathrm{exp}}\Phi_{\mathrm{R}} \\ \gamma_{\mathrm{G}}(n_{\mathrm{G}}) &= T_{\mathrm{exp}}\Phi_{\mathrm{G}} \\ \gamma_{\mathrm{B}}(n_{\mathrm{B}}) &= T_{\mathrm{exp}}\Phi_{\mathrm{B}} \end{aligned} \tag{12}$$

where T_{exp} is the exposure time of the camera. The photometrical response function of a pixel is then defined as the sum of the response functions of each channel multiplied by the corresponding visibility factor

$$\begin{aligned} g(n_{\mathrm{R}}, n_{\mathrm{G}}, n_{\mathrm{B}}) &:= 683^{-1} \\ &\times (V_{\mathrm{R}} \cdot \gamma_{\mathrm{R}}(n_{\mathrm{R}}) + V_{\mathrm{G}} \cdot \gamma_{\mathrm{G}}(n_{\mathrm{G}}) + V_{\mathrm{B}} \cdot \gamma_{\mathrm{B}}(n_{\mathrm{B}})) \end{aligned} \tag{13}$$

with units in lumens $\times$ seconds.

To obtain the behavior of these functions, we have stabilized the following experimental setup shown in Fig. 3. In a dark room, a diffuse light screen source is framed, and its illuminance at distance $b = 17$ cm is measured to obtain different intensity levels. We used a color monitor, with adjustable contrast, brightness, and R, G, B levels, as a light screen

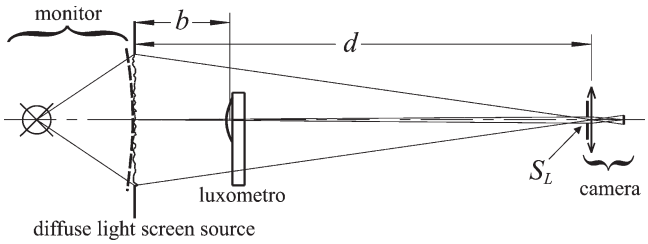

Fig. 3. Experimental setup for the camera calibration.

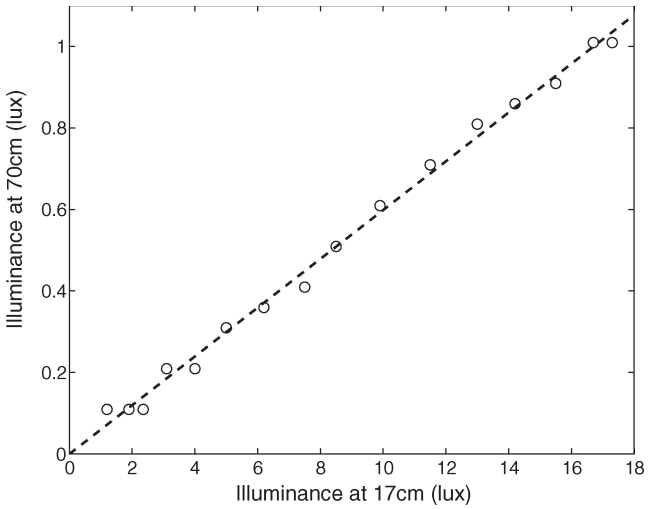

Fig. 4. Linear relation of the illuminance values at different distances from the light source.

source, and we placed a circular field diaphragm, with a diffuser having a diameter of 8 cm, just in front of the monitor. We placed the camera at a distance $d = 70$ cm from the field diaphragm to the first lens of the objective. We also placed a circular diaphragm acting as an entrance pupil, with a diameter $S_{\mathrm{L}} = 5.5$ mm, just in front of the first lens. The illuminance (E_d) on the entrance pupil at a distance d was very low (one lux or smaller) and hardly resolvable with the luxometer used (PCE-172 with a resolution of 0.1 lux).

Thus, we measured the illuminance (E_b) at a closer distance (b) to the screen, and with a linear relation, we relate the illuminance on the entrance pupil to the illuminance E_b. From a few measurements of E_d versus E_b, we obtain the linear adjustment $E_d = 0.0598 \cdot E_b$, as shown in Fig. 4. We have forced the offset to be zero by subtracting it from all E_d values. This offset comes from the background light and has no effect on the camera pixel response. With the luxometer, we then obtain the luminous flux (in lumens) entering the camera from the source screen $F_{\mathrm{L}} = E_d S_{\mathrm{L}}$.

If the image of the luminous screen has a uniform distribution of the $n_{\mathrm{R,G,B}}$ values, the luminous flux impinging on one pixel is then obtained by dividing the total (entering the camera) luminous flux by the number of pixels (N_{imagen}) on which the image of the luminous screen is formed: $F_{\mathrm{p}} = F_d / N_{\mathrm{imagen}}$. By gradually changing the intensity of the light screen source, a set of values of F_{p} versus $n_{\mathrm{R,G,B}}$ is obtained.

Fig. 5(a) shows an image of the light source screen at a certain intensity level and the diagonal where the profile has been taken, and Fig. 5(b) shows several diagonal profiles across

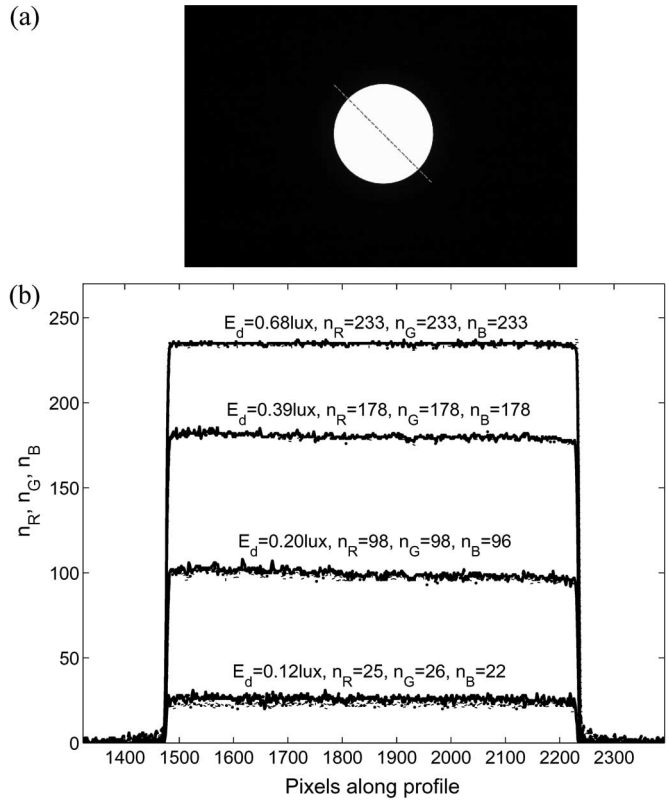

Fig. 5. (a) Image of the light source screen. (b) Profiles along the dashed line shown on image (a) for different intensity levels of the light source. The illuminances at the camera distance are indicated as well as the mean n_{R}, n_{G}, and n_{B} values over the image. The responses of each channel R, G, and B are plotted in solid, dashed, and dotted lines, respectively.

the images of the light screen source at different intensity levels. The number of pixels which forms the image was $N_{\mathrm{imagen}} = 472\,157$, which is the same for all the intensity levels. The $n_{\mathrm{R,G,B}}$ values along the profiles show a quite uniform distribution, and by adjusting the R, G, and B levels of the monitor, we can obtain similar values for n_{R}, n_{G}, and n_{B} for each intensity level, as shown by the profile for each image.

The luminous flux exciting each channel (in watts) is obtained from the values of $n_{\mathrm{R,G,B}}$, the measured luminous flux at a pixel (obtained from the luxometer in lumens), and the visibility factors of each of the primary colors as follows:

$$\Phi_{\mathrm{R}} = \frac{683 \cdot F_{\mathrm{p}} n_{\mathrm{R}}}{V_{\mathrm{R}} n_{\mathrm{R}} + V_{\mathrm{G}} n_{\mathrm{G}} + V_{\mathrm{B}} n_{\mathrm{B}}},$$
$$\Phi_{\mathrm{G}} = \frac{683 \cdot F_{\mathrm{p}} n_{\mathrm{G}}}{V_{\mathrm{R}} n_{\mathrm{R}} + V_{\mathrm{G}} n_{\mathrm{G}} + V_{\mathrm{B}} n_{\mathrm{B}}},$$
$$\Phi_{\mathrm{B}} = \frac{683 \cdot F_{\mathrm{p}} n_{\mathrm{B}}}{V_R n_{\mathrm{R}} + V_{\mathrm{G}} n_{\mathrm{G}} + V_{\mathrm{B}} n_{\mathrm{B}}}. \quad (14)$$

These expressions are obtained with the supposition that the luminous flux at each channel is given by the $n_{\mathrm{R,G,B}}$ values whenever the difference between them is not very big (due to a possible nonlinear response), as in the case of our white light screen source. Then, the total luminous flux at a pixel is

$$\Phi_{\mathrm{p}} = \Phi_{\mathrm{R}} + \Phi_{\mathrm{G}} + \Phi_{\mathrm{B}} = \frac{n_{\mathrm{R}}}{n_{\mathrm{T}}}\Phi_{\mathrm{p}} + \frac{n_{\mathrm{G}}}{n_{\mathrm{T}}}\Phi_{\mathrm{p}} + \frac{n_{\mathrm{B}}}{n_{\mathrm{T}}}\Phi_{\mathrm{p}} \quad (15)$$

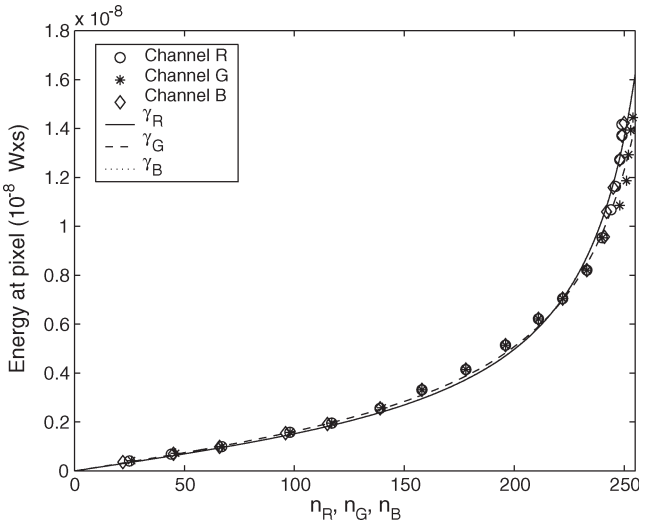

Fig. 6. Luminous energy exciting each channel at a pixel with respect to the channel responses n_{R}, n_{G}, and n_{B}.

TABLE I
RESPONSE FUNCTION COEFFICIENTS OF THE R, G, AND B CHANNELS

	a [W×s]	e
γ_R	$2.437 \cdot 10^{-9}$	$5.576 \cdot 10^{-3}$
γ_G	$2.686 \cdot 10^{-9}$	$5.423 \cdot 10^{-3}$
γ_B	$2.442 \cdot 10^{-9}$	$5.576 \cdot 10^{-3}$

where $n_{\mathrm{T}} = n_{\mathrm{R}} + n_{\mathrm{G}} + n_{\mathrm{B}}$. Φ_{p} can be obtained in dependence of F_{p} with (15) in (11)

$$683 \cdot F_{\mathrm{p}} = (V_{\mathrm{R}} n_{\mathrm{R}} + V_{\mathrm{G}} n_{\mathrm{G}} + V_{\mathrm{B}} n_{\mathrm{B}}) \Phi_{\mathrm{p}} / n_{\mathrm{T}} \qquad (16)$$

and by replacing the obtained Φ_{p} from (16) in (15), we finally obtain (14).

For each measured luminous flux, we then have the $n_{\mathrm{R,G,B}}$ response values of the camera and the ratio of the luminous energy exciting each channel. From the graphical representation of the experimental data shown in Fig. 6 ($T_{\mathrm{exp}} \cdot \Phi_{\mathrm{R,G,B}}$ versus $n_{\mathrm{R,G,B}}$), we obtain the value of the response function for each of the channels for several values of $n_{\mathrm{R,G,B}}$. The total luminous energy at the pixel is the sum of the energy arriving at each channel. The response of each channel results to be clearly nonlinear and has been adjusted with the following tangential function so that it better fits the data in a least squares sense:

$$\gamma_{\mathrm{R,G,B}}(n_{\mathrm{R,G,B}}) = a \tan(e \cdot n_{\mathrm{R,G,B}}), \qquad \text{for } n_{\mathrm{R,G,B}} \leq 255. \qquad (17)$$

The coefficients a and e of the response function of each channel are given in Table I. The saturation energy results in $1.62 \cdot 10^{-8}$ W × s for the R- and B-channels and $1.41 \cdot 10^{-8}$ W × s for the G-channel. The response function of the three channels coincides with the majority of the $n_{\mathrm{R,G,B}}$ values, except for $n_{\mathrm{R,G,B}} > 230$, where the G-channel seems to need less energy to achieve the same response as the R- and B-channels.

TABLE II
LUMINOUS FLUX OF DIFFERENT COLORED LIGHT SCREENS OBTAINED WITH THE LUXOMETER AND THE CAMERA. CAMERA SETTINGS: $f = 55$ mm, $N_f = 1.6$, and $T_{\mathrm{exp}} = 0.5$ s

Light screen color	n_R	n_G	n_B	$F_{p,cam}$ ($\times 10^{-12}$ lm)	$F_{p,lux}$ ($\times 10^{-12}$ lm)
Red	168	24	2	5.63	5.63
Green	27	120	41	5.77	6.28
White Blue	179	224	254	29.17	32.21
White Green	198	233	212	31.70	36.21

Herewith, we obtain the photometrical response function for each channel

$$g_{\mathrm{R,G,B}}(n_{\mathrm{R,G,B}}) = 683^{-1} V_{\mathrm{R,G,B}} \cdot \gamma_{\mathrm{R,G,B}}(n_{\mathrm{R,G,B}}) \qquad (18)$$

for the photometrical response function of a pixel of our camera

$$g(n_{\mathrm{R}}, n_{\mathrm{G}}, n_{\mathrm{B}}) = g_{\mathrm{R}}(n_{\mathrm{R}}) + g_{\mathrm{G}}(n_{\mathrm{G}}) + g_{\mathrm{B}}(n_{\mathrm{B}}). \qquad (19)$$

To obtain the response functions shown in Fig. 6 and their coefficients given in Table I, we need to know the visibility factors of the primary colors. These have been obtained with the help of a minimization process. By varying V_{R}, V_{G}, and V_{B} (with values between zero and one), we minimize the absolute value of the difference between $F_{\mathrm{p,lux}}$ (obtained with the luxometer) and $F_{\mathrm{p,cam}}$ [obtained from the camera using (7), (17), and (18)] of several light screen sources of different colors. We obtain the following: $V_{\mathrm{R}} = 0.490$, $V_{\mathrm{G}} = 0.900$, and $V_{\mathrm{B}} = 0.098$. Table II gives the luminous flux at a pixel (obtained from the luxometer and from the camera) for some color images with their respective $n_{\mathrm{R,G,B}}$ values.

We obtain an acceptable agreement between the $F_{\mathrm{p,lux}}$ and the $F_{\mathrm{p,cam}}$, although the luxometer resolution of ± 0.05 lux introduces an imprecision of the luminous flux at a pixel of $\pm 3 \times 10^{-12}$ lm. With higher light energies, the $F_{\mathrm{p,lux}}$ values are more affected by an imprecision in the slope estimation of the linear relation ($E_d = 0.0598 \cdot E_b$) shown in Fig. 4, explaining the bigger discrepancy between the higher value of $F_{\mathrm{p,lux}}$ with respect to $F_{\mathrm{p,cam}}$ for white–blue and white–green light screen sources.

Fig. 7 shows the photometrical response function, (using the aforementioned estimated visibility factors) with respect to the $n_{\mathrm{R,G,B}}$ values of the corresponding channel and the total photometrical response function, supposing that each channel has the same $n_{\mathrm{R,G,B}}$ value.

The CMOS sensor shows to have a nonlinear response with the luminous energy, but this is not a major disadvantage if we know the response function. The principal reason for using a CMOS sensor instead of a CCD (with high linearity) is that there will be no blooming effects where the exceeding charges of the saturated pixels move to a strip of adjacent pixels in the direction where the charges are collected, introducing an error in the luminance measurements in all the pixels of the strip. The blooming effect easily happens during night-time evaluation of traffic signs where the sensitivity of the camera has been increased, and the bright punctual background light sources are often present.

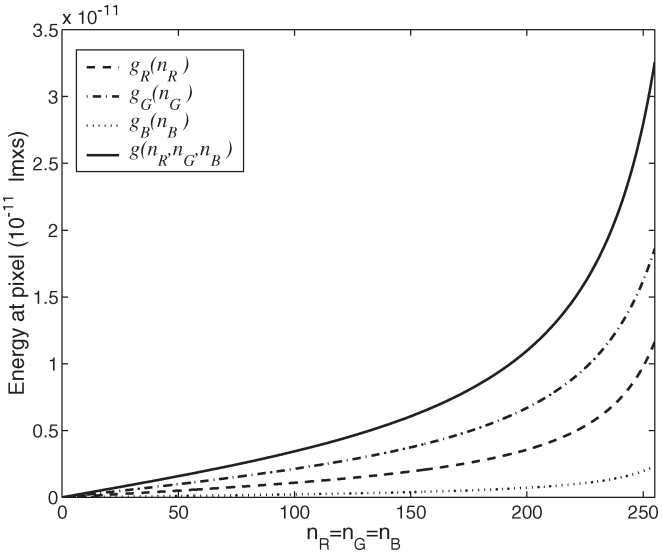

Fig. 7. Photometrical response function at a pixel (total and per channel) with respect to the channel responses n_{R}, n_{G}, and n_{B}.

V. Experimental Results

To prove (9) and (10), we measure the luminance and the retroreflectivity from a vertical traffic sign surface of a circular speed limitation sign with number in black, a white background, and a red rim. We have done two sequences of measurements at different camera–sign surface distances (d) ranging from 5 to 30 m, at night and with two illumination conditions. In the first sequence, we maintained a constant illumination of the sign surface, and in the second sequence, we varied the sign illumination by placing the light source next to the camera so that $d_Q \approx d$ and $\cos\alpha_{\mathrm{i}} \approx \cos\alpha$. Furthermore, the dimensions of the vertical traffic sign (diameter of 0.6 m) are sufficiently smaller than d so that w_{L} and the illuminance are practically the same for each surface element over S. To obtain the reflectivity, we also measured the illuminance on the sign with a luxometer.

The measurement has been done with the photometrical calibrated camera whose objective is focal variable ($f =$ 18 to 55 mm) and where N_f and T_{exp} can manually be set. For simplicity, the image has always been taken in retroreflective conditions and almost normal to the sign surfaces ($\cos\alpha \approx 1$ because of the influence of a slight pavement variation) and with the sign centered on the optical axis of the objective of the camera by centering the image of the sign on the sensor matrix.

In Fig. 8, we show the luminance map of the surface elements of the sign with a constant illumination obtained at three different distances ($d = 5, 17.5$, and 30 m) and with the camera settings $f = 55$ mm, $N_f = 4.5$, and $T_{\mathrm{exp}} = 1/4$ s. The profile across the "zero" [Fig. 8(d)] shows that there is no variation in the measured luminance of the surface elements measured at the different distances because the size of the surface elements (defined as dose whose image is formed on a pixel area) increases with d at the same rate as the luminous flux on the pixel (coming from this surface element) decreases. This behavior is in accordance with (10).

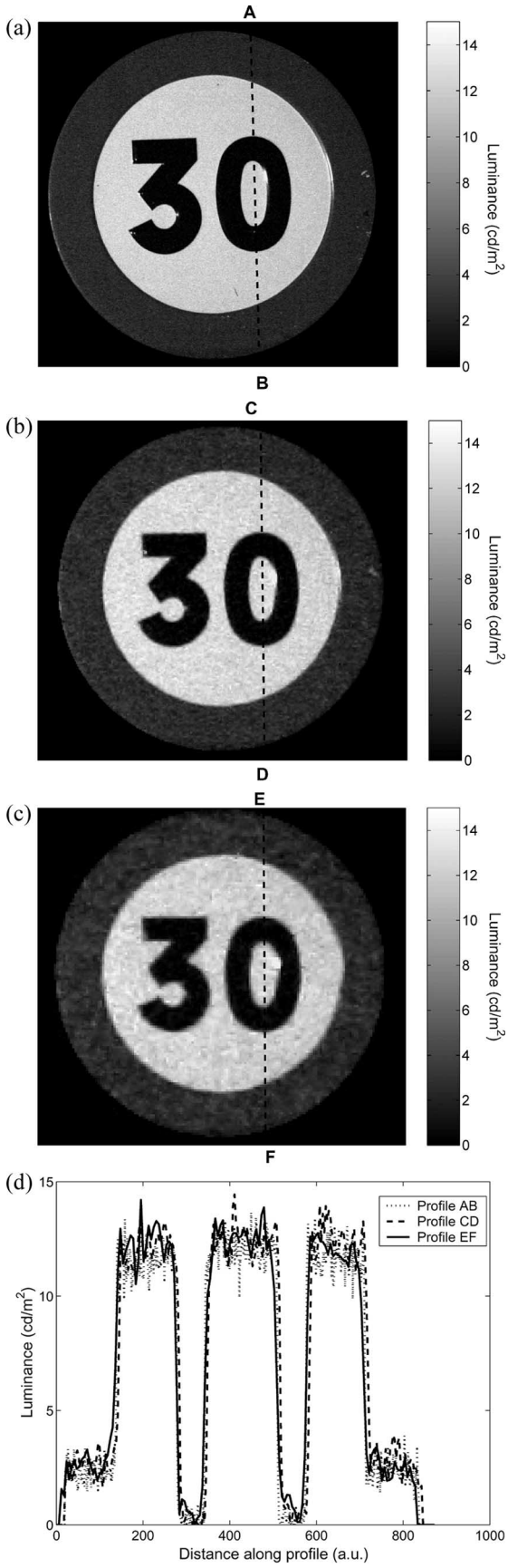

Fig. 8. Luminance map of the surface elements (forming images on the pixels) for different distances of the traffic sign with a constant illumination. (a) $d =$ 5 m. (b) $d = 17.5$ m. (c) $d = 30$ m. (d) Luminance values along the profile shown on the corresponding luminance maps.

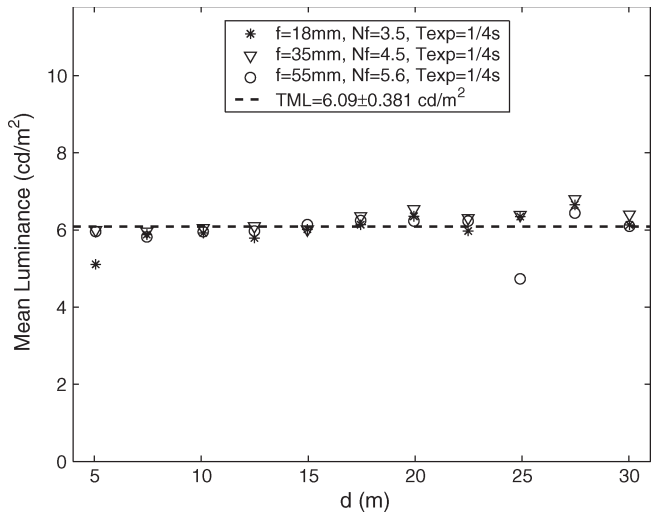

Fig. 9. Mean luminance of the surface elements with a constant illumination of the whole sign at different distances and different camera settings.

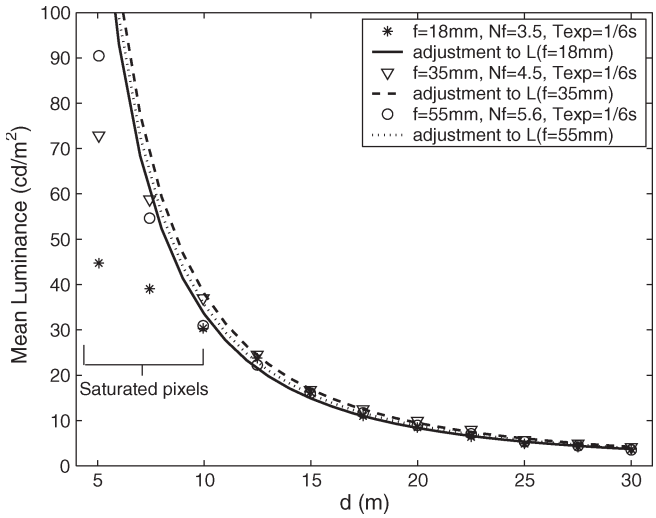

Fig. 10. Mean luminance of the surface elements with a variable illumination of the whole sign at different distances and different camera settings.

To prove both, the constant behavior of the luminance with a constant illumination and its invariance with different camera settings, we took a sequence of 11 measurements at different distances ($d = 5$ to 30 m in intervals of 2.5 m), each of them with different camera settings. The result is shown in Fig. 9 where the mean luminances of the surface elements over the sign surface are represented for different d's. The measurements with $f = 18$ mm, $N_f = 3.5$, and $T_{\text{exp}} = 1/4$ s give a mean value of the mean luminance (and standard deviation) of 6.03 ± 0.377 cd/m^2, the measurements with $f = 35$ mm, $N_f = 4.5$, and $T_{\text{exp}} = 1/4$ s give a mean value of the mean luminance of 6.26 ± 0.254 cd/m^2, and the measurements with $f = 55$ mm, $N_f = 5.6$, and $T_{\text{exp}} = 1/4$ s give a mean value of the mean luminance of 5.98 ± 0.429 cd/m^2. The mean value of the previous mean luminances, which we call the total mean luminance (TML), results in 6.09 ± 0.381 cd/m^2.

The same sequence of 11 images has been taken with variable illumination with a light source placed next to the camera and with the following three camera settings: $f = 18$ mm, $N_f = 3.5, T_{\text{exp}} = 1/6$ s; $f = 35$ mm, $N_f = 4.5, T_{\text{exp}} = 1/6$ s; and $f = 55$ mm, $N_f = 5.6$, $T_{\text{exp}} = 1/6$ s. The mean of the luminance measured at each pixel over the traffic sign image is shown in Fig. 10. For distances of 10 m and smaller, the illuminance of the sign is very high, and an appreciable amount of the pixels of the sign image is saturated (in one or more of the channels), giving an underestimation of the real luminance value at these pixels, and therefore, they are not considered. For higher distances, the illuminance of the sign decays with d^{-2}. A least squares adjustment with the function $L_{\text{adj.}} = m/d^2$ is applied to the data for each of the camera settings and is also shown in Fig. 10. The data give similar adjustments with $m = 3350, 3800,$ and 3560 cd for $f = 18, 35,$ and 55 mm for the three camera settings, respectively, and hence, the three camera settings yield similar values, as shown in Fig. 10.

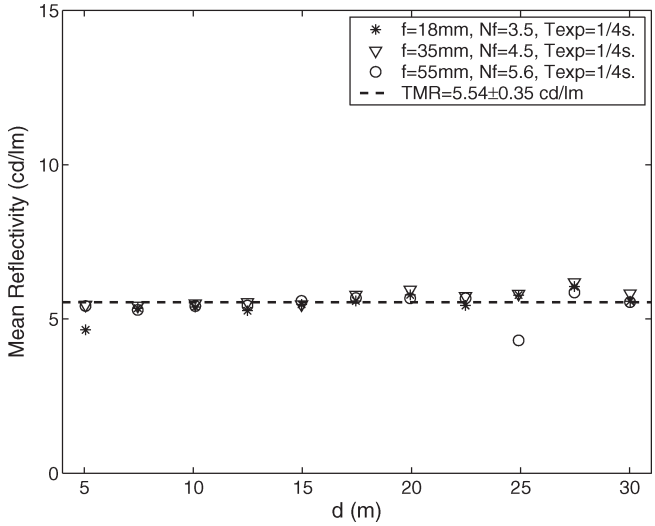

Fig. 11. Mean retroreflectivity of the surface elements with a constant illumination of the whole sign at different distances and different camera settings. The illuminance value of the sign is $E_{\text{i}} = 1.1$ lux.

TABLE III
MEAN VALUE OF THE MEAN RETROREFLECTIVITY (MMR) OF THE SIGN FOR DIFFERENT CAMERA SETTINGS

Camera Settings	MMR with constant illumination. (cd/m^2)	MMR with variable illumination. (cd/m^2)
f=18 mm, N_f=3.5	5.48 ± 0.34	4.96± 0.30
f=35 mm, N_f=4.5	5.69 ± 0.23	5.69± 0.26
f=55 mm, N_f=5.6	5.44 ± 0.39	5.16± 0.20

To prove both, the constant behavior of the luminance with a constant illumination and their invariance with different camera settings, we took a sequence of 11 measurements at different distances ($d = 5$ to 30 m in intervals of 2.5 m), each of them with different camera settings. The result is shown in Fig. 9 where the mean luminances of the surface elements over the sign surface are represented for different d's. The measurements with $f = 18$ mm, $N_f = 3.5$, and $T_{\text{exp}} = 1/4$ s give a mean value of the mean luminance (and standard deviation) of 6.03 ± 0.377 cd/m^2, the measurements with $f = 35$ mm, $N_f = 4.5$, and $T_{\text{exp}} = 1/4$ s give a mean value of the mean luminance of 6.26 ± 0.254 cd/m^2, and the measurements with $f = 55$ mm, $N_f = 5.6$, and $T_{\text{exp}} = 1/4$ s give a mean value of

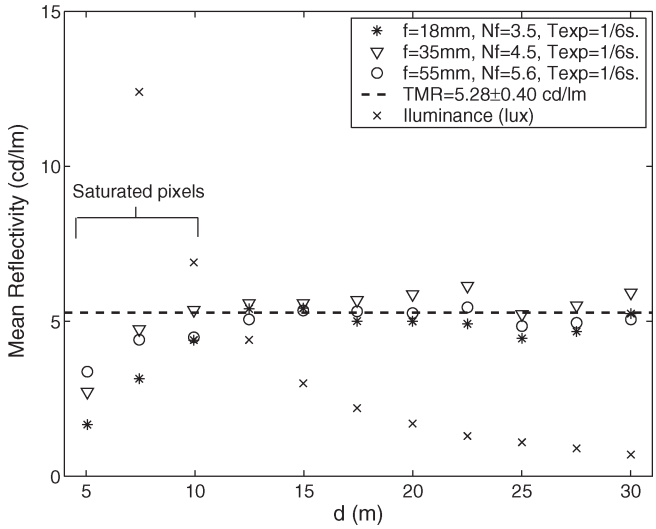

Fig. 12. Mean retroreflectivity of the surface elements with a variable illumination of the whole sign at different distances and different camera settings. The illuminance of the sign varies, as indicated.

the mean luminance of 5.98 ± 0.429 cd/m^2. The TML results in 6.09 ± 0.381 cd/m^2.

The mean retroreflectivity with a constant illumination is obtained by dividing the luminance by the illuminance on the sign ($E_{\mathrm{i}} = 1.1$ lux), and it is therefore also constant. The mean retroreflectivity of the sign for each distance and camera setting is shown in Fig. 11. The total mean retroreflectivity (TMR) results in 5.5 ± 0.35 cd/lm, and the mean values of the mean retroreflectivity (MMR) with a constant illumination for each camera setting are given in Table III.

Fig. 12 shows the mean retroreflectivity with a variable illumination. In this case, the illuminance of the sign varies, as indicated by "$\times$" points on the same figure. The TMR results in 5.3 ± 0.40 cd/lm, and the MMR with a variable illumination for each camera setting are given in Table III.

VI. Conclusion

The experimental results closely coincide with the theory. The luminance and the retroreflectivity remain constant to the distance when the illumination of the sign is constant. The retroreflectivity is shown to be constant, even when varying the distance in the case of variable illumination, and similar values of the TMR are obtained (5.5 ± 0.35 and 5.3 ± 0.40 cd/lm for constant and variable illuminations, respectively).

With different camera settings, we also obtain a high degree of accordance between the MMR, as shown in Table III, where different exposure times for constant and variable illuminations (1/4 and 1/6 s, respectively) have been used, nevertheless obtaining equal results between their MMR and TMR.

This paper provides the basis for an "on road" (while traveling along the road) reflectivity evaluation of the vertical traffic sign with a digital camera: During the day, we may consider a constant illumination, and at night time, we may consider the head lamps of the vehicle as light sources (i.e., variable illumination).

Acknowledgment

The authors would like to thank J. C. Martínez Antón for his valuable suggestions.

References

[1] *Maintaining Traffic Sign Retroreflectivity*, Dec. 2003. FHWA-SA-03-027. [Online]. Available: http://safety.fhwa.dot.gov/roadway_dept/retro/sign/sa03027.htm

[2] D. Beacco, P. Fiorentin, and G. Rossi, "A system for in situ measurements of road reflection properties," in *Proc. IMTC*, Vail, CO, May 20–22, 2003, pp. 1508–1512.

[3] L. Bellia, A. Cesarano, F. Minichiello, and S. Sibilio, "Setting up a CCD photometer for lighting research and design," *Build. Environ.*, vol. 37, no. 11, pp. 1099–1106, Nov. 2002.

[4] G. Rossi, P. Iacomussi, M. Sarotto, and P. Soardo, "CCD matrix detector for photometry," in *Proc. 8th Int. Congr. Metrology*, Besançon, France, Oct. 1997, pp. 326–330.

[5] S. Maldonado-Bascón, S. Lafuente-Arroylo, P. Gil-Jiménez, H. Gómez-Moreno, and F. López-Ferreras, "Road-sign detection and recognition based on support vector machines," *IEEE Trans. Intell. Transp. Syst.*, vol. 8, no. 2, pp. 264–278, Jun. 2007.

[6] P. Fiorentin, P. Iacomussi, and G. Rossi, "Characterization and calibration of a CCD detector for light engineering," *IEEE Trans. Instrum. Meas.*, vol. 54, no. 1, pp. 171–177, Feb. 2005.

[7] R. H. Simons and R. Bean, *Lighting Engineering: Applied Calculations*. Oxford, U.K.: Architectural, 2001, ch. 1, 7.

[8] J. Casas, *Optica*, 7th ed. Zaragoza, Spain: Librería PONS, 1994, ch. 20.

Philip Siegmann received the B.S. degree in physics and the Ph.D. degree in physics in the field of applied optics from the Universidad Complutense de Madrid, Madrid, Spain, in 1998 and 2002, respectively.

From 2003 to 2004, he was a Research Assistant with the Department of Mechanical Engineering, University of Sheffield, Sheffield, U.K. In 2004, he was a Part-Time Optical Designer with the enterprise AOSA S.A., specializing in the supply and design of optical instruments, and a Part-Time Associate Professor with the Escuela Universitaria de Óptica, Madrid. Since 2005, he has been an Associate Professor with the Department of Signal Theory and Communications, Universidad de Alcalá, Alcalá de Henares, Spain. His actual research interests comprise fringe pattern analysis, photometry, and air pollution.

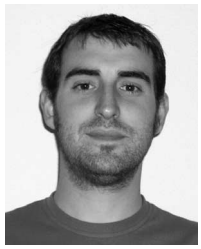

Roberto Javier López-Sastre received the B.S. degree in electrical engineering from the Universidad de Alcalá, Alcalá de Henares, Spain, in 2005, where he is currently working toward the Ph.D. degree within the Department of Signal Theory and Communications.

Pedro Gil-Jiménez received the Telecommunication Engineering degree from the Universidad de Alcalá, Alcalá de Henares, Spain, in 2001.

In 1999, he joined the Department of Signal Theory and Communications, Universidad de Alcalá, where he has been a Lecturer since 2001. His research interests include computer vision, video surveillance systems, and intelligent transportation systems, particularly those involving signal and image processing.

Sergio Lafuente-Arroyo received the B.S. and M.S. degrees in telecommunication engineering from the Universidad de Alcalá, Alcalá de Henares, Spain, in 2000 and 2004, respectively.

He is currently an Instructor with the Department of Signal Theory and Communications, Universidad de Alcalá. His areas of research interest include digital image processing and computer vision.

Saturnino Maldonado-Bascón (M'98) received the B.S. degree in telecommunication engineering from the Universidad Politécnica de Madrid, Madrid, Spain, in 1996 and the Ph.D. degree from the Universidad de Alcalá, Alcalá de Henares, Spain, in 1999.

In 1997, he joined the faculty of the Universidad de Alcalá, where he has been an Associate Professor with the Department of Signal Theory and Communications since 2001. His research interests are image processing and pattern recognition.